Optimization of Wind Farms for Communities

Ahmad Vasel-Be-Hagh[1]

[1]Fluid Mechanics Research Lab, Mechanical Engineering Department,

Tennessee Technological University

2018

Cite as: Vasel-Be-Hagh, Ahmadreza: 'Optimization of wind farms for communities' (Power and Energy, 2018), 'Wind and Solar Based Energy Systems for Communities', Chap. 3, pp. 27-61, DOI: 10.1049/PBPO130E$_{c}h$3.

Abstract

Energy supplies are moving away from environmentally damaging, finite, and expensive fossil fuels to renewable energy resources through technological innovations. Wind energy is one of the most advanced renewable energy resources due to the extensive research that has been ongoing over the last decades to optimize aerodynamic performance of wind turbines, structural design of wind turbines, control strategies, site selection, and the layout of wind farms. This chapter outlines fundamental elements of wind farm layout optimization including optimization parameters, objective functions, wake loss models, and search methods. Optimization parameters include base location, number, rotor diameter, hub height, rotational direction, and yaw angle of wind turbines, as well as shape of wind farm area. In the wake loss models section, all existing wake loss models including large eddy simulation, non-linear and linearized Reynolds-averaged Navier-Stokes models, stochastic models, kinematic models, and empirical models are discussed. In addition, different search methods, from simple greedy search algorithms to advanced genetic algorithms, are briefly reviewed and compared.

1 Introduction

The operational performance of a wind turbine sited in a wind farm - of any scale; either a small onshore community-sized wind farm or a commercial-sized offshore wind farm - is negatively affected by the wake of other wind turbines. Hence, under similar wind conditions, the annual energy production (AEP) of a wind turbine sited in a wind farm is always significantly less than that of an identical single isolated wind turbine. To put this into perspective, the relative power production of a turbine located in the second row of the Norrekaer wind farm, an onshore wind farm in Denmark, is approximately 40-50% of a single isolated turbine under similar free-stream conditions when wind blows along the column of the turbines. Wind farm layout optimization, in its classic definition, is known as optimizing the position of wind turbines in order to minimize the above-described negative wake effect. In more advanced and inclusive analyses, however, several other characteristics of the wind farm, including, number of turbines [1, 2], rotor diameter (i.e. turbine type) [3, 4], hub height [5, 6, 7, 8, 3, 9, 10], rotational direction [11], and length of power transmission lines [12, 13, 14, 15, 16, 17, 18, 19, 20] are determined simultaneously with the position of wind turbines in order to optimize the annual energy production of the wind farm, the environmental impacts, and the economic benefits.

The process of optimizing the layout of a wind farm consists of two major steps (Fig. 1). First, a search algorithm is required to identify all possible layouts over the given wind farm area. Second, a wake-loss model is required to predict the power production of the layout identified in the first step. Depending on the way through which the interaction between these two steps are defined, optimization techniques can be classified as one-way or two-way algorithms.

In optimization algorithms with the one-way structure, the search process is independent of the power prediction step. The search algorithm identifies a layout, and then, the power

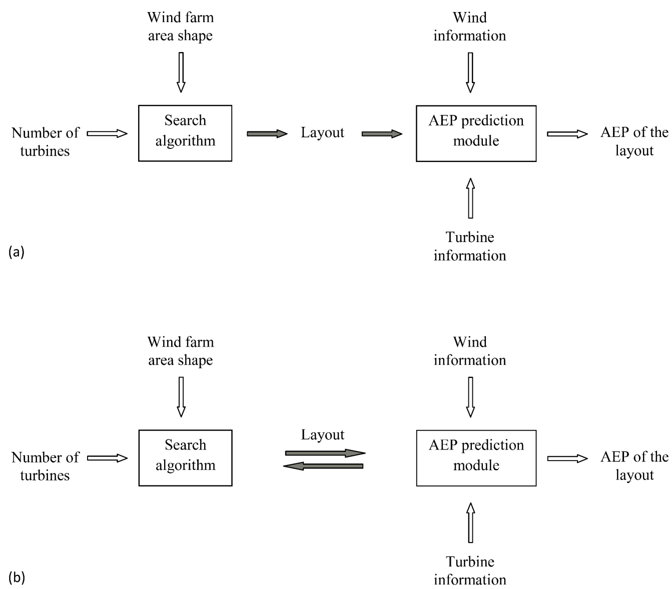

Figure 1: Wind farm layout optimization algorithm with (a) a one-way structure and (b) a two-way structure.

production of the identified layout is predicted and stored by the power prediction module of the optimization algorithm (Fig. 1(a)). Once the search is completed, the layout with the maximum power (or maximum AEP) is selected as the optimal layout. One example of a one-way optimization structure is the algorithm developed by Ghaisas and Archer [21]. They described a wind farm layout using four independent design parameters defined as the spacing between consecutive turbines in the X-direction (SX), the spacing between consecutive turbines in the Y-direction (SY), the staggering of alternate rows in the Y-direction (SDY), and the angle between rows and columns (β). Then, hundreds of layouts are identified by assigning ranges of values to those discrete design parameters (i.e., SX, SY, SDY, and β) and power production of each layout is predicted using Geometric Models. Finally, the layout with highest power production is chosen as the optimal layout. During this exhaustive search for identifying possible layouts no information is communicated between the search and the power prediction modules and all of the layouts are identified upfront.

In optimization algorithms with a two-way structure, however, the search algorithm constantly communicates with the power prediction module and modifies the search process accordingly (Fig. 1(b)). Hence, the two-way optimization algorithms are more sophisticated; however, they are smarter and are able to identify more efficient optimal layouts in a shorter period of time. For instance, in the optimization algorithm developed by Vasel-Be-Hagh and Archer [5], first, a turbine-placement grid with N_g grid points is mapped onto the wind farm area, and the optimization algorithm is initialized by placing one turbine at one of the grid points. Then, the second turbine is placed at all $(N_g - 1)$ available locations one by one to determine the base location for which AEP of the two placed turbines is maximized. This procedure continues until n reaches N_T, where N_T is the total number of turbines. This dynamic programming approach identifies the optimal layout by adding one turbine at a time according to the information that is being communicated between the search and the power prediction modules.

In this chapter, first all optimization variables and objective functions that need to be taken into account to develop an efficient design for a community-sized wind farm are discussed (§2). Then, different kinds of wake-loss models that have been introduced in literature in order to predict power production of a given wind farm are presented (§3). Finally, available search algorithms that have been developed for wind farm layout optimization purposes are presented and discussed (§4).

2 Objective functions and optimization variables

Wind farm layout optimization includes identifying not only the optimal positions for the turbines to maximize the power or the annual energy production of the wind farm, but also the optimal hub height, the optimal number of turbines, the optimal rotational direction, and the optimal rotor diameter (i.e., turbine type) to minimize the levelized cost of energy, to minimize the adverse environmental impacts such as noise production, and to minimize

Table 1: Objective functions considered for wind farm design and developement.

Objective functions	Objective	Literature
Annual Energy Production (AEP)	Maximizing	[22? , 18, 35? , 84?]
Power Production (PP)	Maximizing	[6, 23, 13, 24, 25, 26, 27, 28]
Levelized Cost of Energy (LCOE)	Minimizing	[2, 29, 23, 30, 31, 32, 33, 34, 35]
		[36, 12, 37, 38, 39, 40, 41, 42, 43]
Net Present Value (NPV)	Maximizing	[44? ? ?]
Noise Propagation (NP)	Minimizing	[2, 1, 45, 46, 47]
Loads Acting on Wind Turbines (WTL)	Minimizing	[24, 23, 48]

the fatigue loads acting on the wind turbines. In this section, all of these objective functions and optimization variables are introduced and discussed in details.

2.1 Objective functions

A list of the most essential objective functions that are required to be optimized in order to develop an efficient design for a commercial-sized wind farm is presented in Table 1. Among all, the annual energy production of the wind farm is the most critical objective function in a wind farm layout optimization analysis. The annual energy production of a wind farm is calculated as,

$$\begin{aligned} AEP = \sum_{i=1}^{360}[fr_i \times (\sum_{j=1}^{n_1}[p_w(u_j)P_c(u_j)\sum_{k=1}^{n_t}[P_{rel(k,i)}]]+ \\ \sum_{j=n_1}^{n_2}[p_w(u_j)P_{rated}N_T]) \times n_h] \end{aligned} \tag{1}$$

where fr_i is the relative frequency of wind in direction i, $p_w(u_j)$ is the probability of having wind at speed of $u_j = (0.5 + j)du$ in direction i and is calculated via Weibull distribution $\big($Eq. (2)$\big)$, du is the wind speed resolution, $P_c(u_j)$ is the power obtained from the power curve of wind turbine at wind speed of u_j, P_{rated} is the rated power of wind turbines, n_1 and n_2 are respectively defined as $n_1 = 1 + u_{rated}/du$ and $n_2 = u_{cut-out}/du$, P_{rel} is the relative power calculated via a wake-loss model, and $n_h = 8760$ denotes number of hours per year. The Weibull distribution, used in Eq. (1) to represent the wind velocity probability density ranging from the cut-in to the cut-out wind speeds, is defined as,

$$P_w(u)du = (\frac{k_w}{c_w})(\frac{u}{c_w})^{k_w-1}exp[-(\frac{u}{c_w})^{k_w}]du, \tag{2}$$

in which P_w, u, k_w and c_w are probability density, wind speed, shape factor, and scale factor respectively.

In many of the wind farm optimization studies, the farm-averaged power production of the wind farm, defined as the total power production of the farm divided by the total number of turbines, is simply used as the objective function of the optimization analysis. It is important to note that a wind farm optimized by maximizing its power production is not necessarily identical to the optimal layout which is obtained based on maximizing the annual energy production, and as the annual energy production is what really matters as the total output of a wind farm, it is recommended to use the annual energy production as the main objective function of the wind farm layout optimization analysis.

Another popular objective of wind farm layout optimization algorithms is minimizing the Levelized Cost of Energy (LCOE) [$/kWh]. In general, the levelized cost of energy is defined as the average total cost to build and operate a wind farm over its lifetime divided by the total energy output of the wind farm over that period of time. Accordingly, the levelized cost of energy is calculated as,

$$LCOE = \frac{C_{Inv}}{aE_a} + \frac{C_{O\&M}}{E_a} \tag{3}$$

where $C_{Inv} = C_{RNA} + C_{SS} + C_{Elect} + C_{Decom}$ is the capital cost in which C_{RNA} is the Rotor-Nacelle Assemblies costs, C_{SS} includes the the support and the structure costs, C_{Elct} denotes the electrical interconnection costs, C_{Decom} is the decommissioning cost, $C_{O\&M}$ is the operational and maintenance costs, and a is the annuity factor defined as

$$a = (1 - (1/(1+r))^T)/r \tag{4}$$

where T is the lifetime of the wind farm in years and r is the interest rate in [%] and is defined as the summation of discount rate and inflation rate. In Eq. (3), E_a is the net effective expected electrical energy of the wind farm and is defined as,

$$E_a = [\sum_{i=1}^{N_T}(E_{WT,i} - E_{WL,i} - E_{CL,i}) - E_{LT}] \tag{5}$$

where $E_{WT,i}$ is the maximum possible energy production of turbine i assuming that turbine i is a front-row turbine, $E_{WL,i}$ is the energy that turbine i loses due to wake effects, $E_{CL,i}$ stands for the energy that turbine i loses through the collection cables, and E_{LT} is the energy loss through the transmission cables.

If the interest rate is low, then it is more efficient to use the Net Present Value (NPV) instead of the Levelized Cost of Energy (LCE) as the objective function for a wind farm layout optimization. The NPV is defined to take into account the fact that a given amount of money is more valuable now than it will be in the future as it can be used now to make more money in the future. The NPV is defined as,

$$NPV = \frac{P_1}{(1+r)^1} + \frac{P_2}{(1+r)^2} + ... + \frac{P_n}{(1+r)^n} \tag{6}$$

in which r is the rate of interest and must be given as a decimal (not percent) and P_i stands for the yearly payment of the i^{th} year.

The noise created by a community wind farm, which is located near residential areas, may be annoying to people living nearby, hence, the layout of those wind farms must be developed so that the noise level of the farm is minimized. Noise created by wind farms has two different sources; first, the aerodynamic noise produced by the blades of turbines cutting through the air on their downward motion, and second, noise made by the gearbox system. Employing thiner blades and shifting to direct drive (i.e., gear-less) wind turbine technologies are efficient approaches to reduce noise of wind turbines at the manufacturing stage. At the wind farm design and development stage, however, the total noise production of a wind farm can be reduced by smart placement of wind turbines. In community wind projects, turbines are normally placed in the wind farm based on a trade-off between maximizing the annual energy production of the wind farm and minimizing its noise propagation. The noise calculations are usually conducted based on the International Standard ISO 9613 which includes a general method of calculation for attenuation of sound during propagation outdoors. Accordingly, sound pressure level of each wind turbine at each receptor location is calculated as

$$L_p = L_w + D_c - A_f \tag{7}$$

where $L_w = 100$ db [1] is sound power level, D_c stands for directivity correction in dB if the source does not emit sound equally in all directions, A_f is the octave-band attenuation defined as

$$A_f = A_{div} + A_{atm} + A_{gr} + A_{bar} + A_{misc} \tag{8}$$

in which A_{div} is the attenuation due to geometrical spreading, A_{atm} is the attenuation due to air absorption, A_{gr} is the attenuation due to ground absorption and reflection, A_{bar} is the free field diffraction attenuation of a barrier, and A_{misc} is the attenuation due to miscellaneous effects such as weather variability and dispersion through complex acoustical structures. International Energy Agency (IEA) has provided the following approximation for Eq. (7),

$$L_p(d_{ir}) = L_w - 10 \times log(2\Pi d_{ir}^2) - \alpha d_{ir} \tag{9}$$

where the indices i and r represent turbine and receptor, d is the distance between turbine and receptor, and $\alpha = 0.005\ db/m$ is a constant. Individual sound pressure levels calculated via Eq. (9) are then summed up using the following equation,

$$L_{p,avg} = 10 \times log\Big(\sum_{i=1}^{ns}\Big(\sum_{j=1}^{8} 10^{0.1(L_p(i,j)+A_f(i,j))}\Big)\Big), \tag{10}$$

in which ns is number of sound sources (i.e., number of turbines), $L_p(i, j)$ is the individual sound pressure level associated with turbine i and octave band j.

Finally, minimizing the fatigue loads acting on the structure of wind turbines can be considered as another objective function for wind farm layout optimization analyses as the damage equivalent loads in a wind farm are highly affected by partial wake overlap and can be significantly decreased by smart placement of turbines and smart handeling of yaw-misalignment [24, 23, 48].

2.2 Optimization variables

If changing the value of a parameter simultaneously exerts a positive and a negative effect on the objective function of a problem, then that parameter can be considered as an optimization variable and there might be an optimal value for it. The most popular optimization variables for wind farm layout optimization analyses is presented in Table 2.

For instance, by lowering the the hub height of the downstream wind turbine by a specific length equal to $k \times d$, where k is the decay coefficient (k=0.04 and 0.078 for offshore and onshore wind farms respectively) and d is the axial distance between the turbines, the downstream wind turbine starts to become unexposed to the upstream wake (see Fig. 2). This *positively* affects the power production of the downstream wind turbine. On the other hand, due to the shear effect, lowering the hub height of the downstream wind turbine causes a reduction in the speed of the wind experienced by this wind turbine, which *negatively* affects its power production. Due to this simultaneous positive and negative effects that are

Table 2: Optimization variables considered for wind farm design and development.

Optimization variables	Studies
Turbine positions	[49, 50, 29, 18, 51, 12, 52, 53, 54?]
Number of turbines	[13, 55, 42, 1, 56]
Rotor diameter	[3, 4]
Hub height	[6, 57, 5, 8, 4]
Electrical Cable Length	[12, 13? , 15, 16, 17, 18? , 20]
Rotational direction	[11]
Wind farm area	[58, 37, 59, 46, 60]

brought about by variation of the hub height of the downwind turbine, the “hub height" can be considered as an optimization variable, and in fact, in many cases, a compromise between the two negative and positive effects can be reached so that the maximum power production of the downstream wind turbine can be achieved at a height lower than the hub height of the upstream wind turbine. Building the downstream wind turbine at this optimal hub height not only increases the power production, but also slightly decreases the average height of the wind farm leading to a reduction of the capital and the maintenance costs [5].

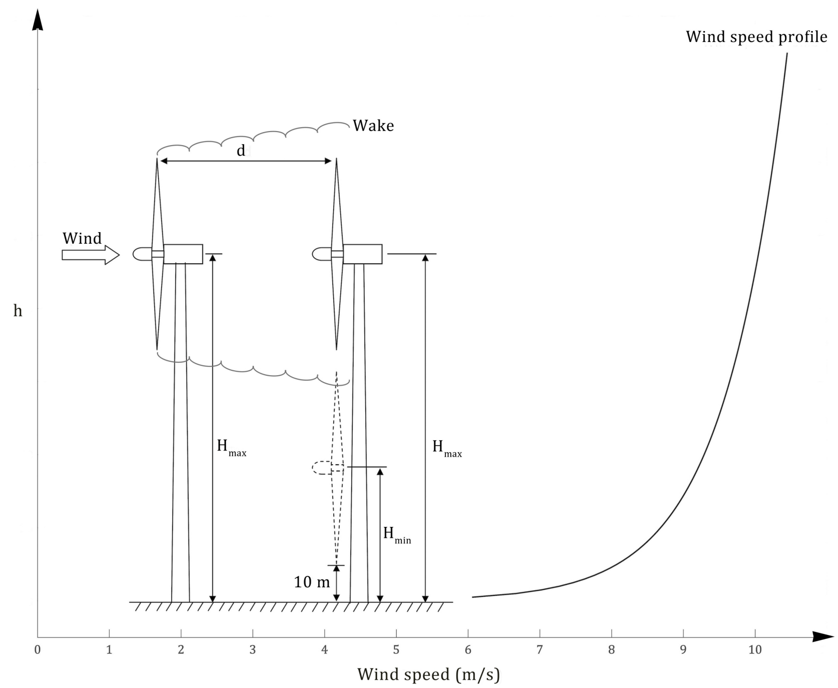

Figure 2: Two in-line wind turbines aligned with the wind direction. The upstream turbine is placed at H_{max} while the hub height of the downstream turbine may vary from H_{max} to H_{min} [5].

Table 3: The most popular wake loss models used in wind energy applications.

Wake loss models	
Large Eddy Simulations (LES):	
	- LES with actuator lines
	- LES with actuator disks
Non-Linear Reynolds-Averaged Navier-Stokes (RANS) Models:	
	- K-ϵ with actuator lines/disks
	- K-ω with actuator lines/disks
Stochastic Models	
Linearized RANS Models:	
	- Ainslie
	- Fuga
Kinematic (Analytical) Models:	
	- PARK (Jensen)
	- Bastankhah / Porte Agel (BPA)
	- Xie / Archer
	- Geometric Model
	- Frandsen
	- Larsen
Experimental Models:	- Ishihara

3 Wake-loss models

A list of the most popular wake loss models used for wind farm design and development purposes is provided in Table 3. These models are described in detail in the following sections.

3.1 Large eddy simulations (LES)

3.1.1 Governing equations

Large eddy simulations govern dynamics of large eddies by removing those with scales smaller than a filter width from the unsteady Navier-Stokes equations and modeling their effects using a subgrid scale model. The filter width is defined as $\Delta = \sqrt[3]{\Delta x \Delta y \Delta z}$ where Δx, Δy, and Δz are cell sizes in the x, y and z directions respectively. The incompressible formulations of the filtered continuity and momentum equations are as follows:

$$\frac{\partial \bar{u}_i}{\partial x_i} = 0 \tag{11}$$

$$\frac{\partial \bar{u}_i}{\partial t} + \frac{\partial \bar{u}_i \bar{u}_j}{\partial x_j} = -\frac{\partial \hat{p}}{\partial x_i} - \frac{\partial \tau_{ij}^D}{\partial x_j} - \frac{1}{\rho_0}\frac{\partial p_0(x,y)}{\partial x_i} + F_{ext} \tag{12}$$

where the bar denotes spatially resolved components; i, j, and k are the indices of the three spatial components x, y and z; u is the wind speed; t is time; $\hat{p}$ is the modified pressure defined as $[\bar{p}(x,y,z,t)/\rho_0 - p_0(x,y)/\rho_0 + \rho_0 gz/\rho_0 + (\tau_{kk})/3]$; p and p_0 are the static and mean pressure; ρ_0 is the reference air density; τ_{ij}^D is the traceless part of the wind stress tensor; and F_{ext} stands for the external forces applied to the wind, including those induced by the wind turbines. According to the Boussinesq eddy viscosity assumption, the traceless stress tensor τ_{ij}^D given in Eq. (12) is defined as

$$\tau_{ij}^D = -2\nu_t \bar{S}_{ij} \tag{13}$$

in which the kinematic eddy viscosity ν_t is defined using the subgrid scale model proposed by Smagorinsky [61] as,

$$\nu_t = (c_s \Delta)^2 |\bar{S}| \tag{14}$$

where $c_s = 0.168$ is the Smagorinsky constant, $\bar{S}_{ij} = (\partial \bar{u}_i/\partial x_j + \partial \bar{u}_j/\partial x_i)/2$ is the filtered strain rate tensor, and $|\bar{S}| = \sqrt{2\bar{S}_{ij}\bar{S}_{ij}}$ is the norm of the filtered strain rate tensor. The external force F_{ext} term in Eq. (12) includes the Coriolis force, the buoyancy force, and the force exerted by turbine blades that is calculated using the actuator line model presented in section 3.1.2. Accordingly, the external force F_{ext} can be expressed as,

$$F_{ext} = \frac{1}{\rho_0} F_i + g(\frac{\bar{\theta} - \theta_0}{\theta_0})\delta_{i3} - \epsilon_{i3k} f \bar{u}_k \tag{15}$$

where F_i is the force generated by the actuator line model, ϵ_{ijk} is the alternating unit tensor, g stands for the gravitational acceleration, θ is the potential temperature, $\theta_0 = 300K$ is the reference temperature, δ_{ij} is the Kronecker delta, and f is the Coriolis parameter defined as $f = 2\Omega sin\phi$ in which Ω is the Earth rotational speed ($\sim 2.95 \times 10^{-5}$ rad/s), and ϕ is the site latitude. The following potential temperature equation needs to be solved coupled with Eqs. (11) and (12) to obtain the potential temperature needed to calculate the buoyancy term in Eq. (15),

$$\frac{\partial \bar{\theta}}{\partial t} + \frac{\partial (\bar{u}_j \bar{\theta})}{\partial x_j} = \frac{\partial q_j}{\partial x_j} \tag{16}$$

where q_j represents the temperature flux defined as

$$q_j = -\frac{\nu_t}{Pr_t} \frac{\partial \bar{\theta}}{\partial x_j}, \tag{17}$$

and Pr_t is the subgrid turbulent Prandtl number defined as [62],

$$Pr_t = \frac{1}{1 + 2\frac{l}{\Delta}} \tag{18}$$

in which,

$$l = \begin{cases} min(7.6\frac{\nu_t}{\Delta}(s^{-\frac{1}{2}}), \Delta) & \text{if } \ s > 0 \\ \Delta & \text{if } \ s \leq 0 \end{cases} \tag{19}$$

and,

$$s = \frac{g}{\theta_0} \frac{\partial \bar{\theta}}{\partial z}. \tag{20}$$

Usually $l = \Delta$, and hence, $Pr_t = \frac{1}{3}$.

3.1.2 The actuator line model

The actuator line modeling, proposed by Sørensen and Shen [63], are usually employed along with large eddy simulations to model the effect of wind turbines. In this model, the turbine blades are represented by three rotating lines that are discretized into N_{be} blade elements with centers located at (x_n, y_n, z_n). N_{be} is recommended to be at least 40. Using airfoil lookup tables, the aerodynamic forces are calculated for each blade element $f_i^a(x_n, y_n, z_n, t)$. Summation of the aerodynamic forces of blade elements corrected via a regularization kernel yields the body force exerted by the blades onto the flow field,

$$F_i = \sum_{n=1}^{40} \frac{f_i^a(x_n, y_n, z_n, t)}{\pi^{3/2}\varepsilon^3} exp[-(\frac{r_n}{\varepsilon})^2], \tag{21}$$

where $f_i^a(x_n, y_n, z_n, t)$ is the actuator element force, F_i is the force field projected as a body force onto CFD grid, r_n is the distance between CFD cell center and the blade element, and ε is used to control the Gaussian width so that it spans from the leading edge to the trailing edge of the blade elements. The value of ε is recommended to be $l_c/4.3$, where l_c indicates the chord length of the blade elements, so at both trailing and leading edges (i.e. $r_n = l_c/2$) the exponential term is reduced to approximately 1% of its maximum [64]. The power calculations are based on the aerodynamic torque that is exerted on the blades. Multiplying the aerodynamic torque by the rotational speed of the rotor yields the power output.

3.2 Nonlinear Reynolds-averaged Navier-Stokes (RANS) models

3.2.1 Governing equations

The continuity and the momentum equations using the Reynolds-averaged Navier-Stokes (RANS) decomposition are as follows,

$$\frac{\partial U_i}{\partial x_i} = 0 \tag{22}$$

$$\rho U_j \frac{\partial U_i}{\partial x_j} = -\frac{\partial P}{\partial x_i} + \frac{\partial}{\partial x_j}\Big[\mu\Big(\frac{\partial U_i}{\partial x_j} + \frac{\partial U_j}{\partial x_i}\Big)\Big] + \frac{\partial}{\partial x_j}\Big[\mu_t\Big(\frac{\partial U_i}{\partial x_j} + \frac{\partial U_j}{\partial x_i}\Big)\Big] + F_{ext} \tag{23}$$

in which μ_t is turbulent viscosity and is defined using a two-equation closure model, such as the $k-\epsilon$ or the $k-\omega$ models. Turbulent viscosity in the $k-\epsilon$ model is defined as,

$$\mu_t = \rho C_\nu \frac{k^2}{\epsilon} \tag{24}$$

where k and ϵ are turbulent kinetic energy and the kinetic energy dissipation rate respectively. The transport equations for k and ϵ are,

$$u_i \frac{\partial k}{\partial x_i} = \frac{\partial}{\partial x_i}\Big[\Big(\nu + \frac{\nu_t}{\sigma_k}\Big)\frac{\partial k}{\partial x_i}\Big] + \nu_t\Big(\frac{\partial u_i}{\partial x_j} + \frac{\partial u_j}{\partial x_i}\Big)\frac{\partial u_i}{\partial x_j} - \epsilon \tag{25}$$

$$u_i \frac{\partial \epsilon}{\partial x_i} = \frac{\partial}{\partial x_j}\Big[\Big(\nu + \frac{\nu_t}{\sigma_\epsilon}\Big)\frac{\partial \epsilon}{\partial x_i}\Big] + C_{\epsilon 1} P_k \frac{\epsilon}{K} - C_{\epsilon 2}\frac{\epsilon^2}{k} \tag{26}$$

where C_ν, $C_{\epsilon 1}$ and $C_{\epsilon 2}$ are the standard model constants and (σ_k, σ_ϵ) are the turbulent Prandtl numbers for k and ϵ respectively. In Eq. (23), F_{ext} stands for the external forces applied to the wind, including those induced by the wind turbines. Wind turbine forces can be modeled through the actuator line model described in section 3.1.2, or using the actuator disk model described in the following section.

3.2.2 The actuator disk model

In the actuator disk model, the wind turbine rotor is modeled as a disk with a diameter equal to the rotor diameter of the real wind turbine and a depth equal to the thickness of the blades. The F_{ext} is then defined as,

$$F_{ext} = \frac{1}{2}\frac{\rho C_T U_0^2}{\Delta x} \tag{27}$$

where U_0 is the inlet velocity at hub height level, Δx stands for the control volume length and is equal to the actuator disk thickness, and C_T is the thrust coefficient defined as,

$$C_T = \frac{T}{\frac{1}{2}\rho U_\infty^2 A_D} \tag{28}$$

in which U_∞ is free stream wind speed, $A_D = \pi D^2/4$ stands for the rotor swept area, and T is the thrust force and is a function of lift (C_L) and drag (C_D) coefficients obtained through airfoil lookup tables.

3.3 Stochastic models

The stochastic models are introduced to fill the gap between the accurate, however, computationally expensive CFD-based models and less accurate, however, computationally efficient analytical models. One of the most effective stochastic models is the wake model proposed by Doubrawa et al. [65] based on large eddy simulations of an offshore wind farm. The proposed stochastic model was found to successfully reproduce the mean characteristics of the original LES wake, including its area and stretching patterns, statistics of the mean azimuthal radius, the mean and standard deviation of the wake width and height, and the velocity deficit and meandering. In this model, the cross section of the wake is defined as a series of wake radius versus azimuth $r_w(\theta)$, where θ is the azimuth angle with respect to the vertical direction and r_w is the distance between the center of the wake from the boundary of the wake at the azimuth angle of θ. The r_w is then decomposed into $\langle r_w \rangle$ and r'_w as $r_w = \langle r_w \rangle + r'_w$ in which $\langle r_w \rangle$ is the azimuthal mean radius and r'_w stands for radii perturbations. At each iteration, $\langle r_w \rangle$ is estimated using stochastic methods and r'_w is obtained using spectral analysis. The azimuthal mean radius $\langle r_w \rangle$ is further decomposed into a constant temporal mean $\overline{\langle r_w \rangle}$ and a dynamic perturbation $\langle r_w \rangle'$ around the constant temporal mean. The values of $\overline{\langle r_w \rangle}$ are extracted upfront from the LES and will be provided by the user as initial conditions of the wake simulator. These values are given in [65] for different distances downstream of turbines. The perturbations $\langle r_w \rangle'$, however, are obtained at every time step through a first-order auto-regressive model as,

$$\langle r_w \rangle'_t = \rho_1 \langle r_w \rangle'_{t-1} + \epsilon(t) \tag{29}$$

where $\rho_1 = 0.9$ is the first-order auto-correlation for the $\langle r_w \rangle'$ time series obtained from the LES data which was found to be approximately the same for different distances downstream, and $\epsilon(t)$ are the random innovations in the form of white noise that make up the time series variability. These innovations are randomly sampled from a normal distribution of mean $\mu = 0$ and standard deviation $\sigma = 0.05R$ which were determined based on the original LES time series of wake radii. More information on stochastic wake models can be found on [66, 67].

3.4 Linearized RANS models

3.4.1 Ainslie model

Ainslie wake model, proposed by Ainslie [68], is a two-dimensional model based on the assumptions that wake of a wind turbine is axisymmetric and pressure gradients are negligible in the wake region. The continuity and momentum equations in free stream direction and in cylindrical coordinates are as follows,

$$\frac{1}{r}\frac{\partial(rv)}{\partial r} + \frac{\partial u}{\partial x} = 0 \tag{30}$$

$$u\frac{\partial u}{\partial x} + v\frac{\partial u}{\partial r} = -\frac{1}{r}\frac{\partial(r\overline{u'v'})}{\partial r} \tag{31}$$

where,

$$-\overline{u'v'} = \epsilon(x)\frac{\partial u}{\partial r} \tag{32}$$

where ϵ is eddy viscosity and is assumed to be a function of distance downstream of the wind turbine. Ainslie decomposed the eddy viscosity term into the ambient eddy viscosity of the atmosphere and the eddy viscosity generated by the wake as,

$$\epsilon(x) = \epsilon_a + \epsilon_w(x) = \epsilon_a + kb\big(U_\infty - u_c(x)\big) \tag{33}$$

in which k is constant and is empirically found to be 0.015, and b is the wake width and is defined as follows based on wind tunnel data,

$$b = \sqrt{\frac{3.56C_T}{4(U_\infty - u_c)(2-(U_\infty - u_c))}} \tag{34}$$

where u_c is wind speed at the centerline of the wake. The Ainslie model is not valid in the near wake area (within 2D from downwind of the rotor), and the following Gaussian velocity profile is used as a boundary condition at x=2D,

$$1 - \frac{u(r)}{U_\infty} = (U_\infty - u_c)exp\Big(-3.56\big(\frac{r}{b}\big)^2\Big) \tag{35}$$

where u is the wind speed at radial distance r with respect to the center line and axial distance $x = 2D$ downwind of the wind turbine. The initial wind speed deficit at the centerline of the wake is,

$$U_\infty - u_c = C_T - 0.05 - (16C_T - 0.5)\frac{I}{10} \tag{36}$$

where I is the ambient turbulence intensity.

3.4.2 Fuga model

Ott et al. [69] developed a linear RANS model called Fuga by employing a very simple closure instead of the one introduced through Eq. (24) to Eq. (26) in the $k - \epsilon$ model. According to the Fuga model,

$$\mu_t = \rho k u^* z \tag{37}$$

where $k = 0.4$ is the Von Karman constant, z is the height from the surface, and u^* is the shear velocity defined as $u^* = \sqrt{\tau/\rho}$ in which τ is the surface shear stress.

3.5 Empirical wake models

There are several wake loss models that are based on experimental data, such as the Ishihara model developed by Ishihara et al. [70] by using wind tunnel data for a scaled model and assuming a Gaussian velocity profile. The wind speed deficit in the Ishihara model is given by,

$$U_\infty - u = \frac{\sqrt{C_T}U_\infty}{32}\Big(\frac{1.666}{k_1}\Big)^2\Big(\frac{x}{D}\Big)^{-p} exp\Big(-\frac{r^2}{D_w^2}\Big) \tag{38}$$

where D_w is the wake diameter defined as,

$$D_w = \frac{k_1 C_T^{0.25}}{0.833} D^{1-0.5p} x^{0.5p} \tag{39}$$

in which p is defined as,

$$p = k_2(I_a + I_w) \tag{40}$$

where I_a and I_w are the ambient turbulence intensity and the turbulence intensity induced by the wind turbines respectively. I_w is estimated as,

$$I_w = \frac{k_3 C_T}{max(I_a, 0.03)}\Big(1 - exp\Big(\frac{-x^2}{25D^2}\Big)\Big), \tag{41}$$

and coefficients k_1, k_2, and k_3 are 0.27, 6, and 0.004 respectively.

3.6 Kinematic (analytical) models

The six most popular kinematic wake models, also called analytical wake models, which have been developed for wind energy applications are PARK (Jensen), Xie-Archer (XA), Bastankhah and Porte-Agel (BPA), Larsen, Frandsen and Geometric Model (GM). These models are respectively described in the following sections.

3.6.1 PARK

The PARK model, developed by Jensen [71, 72], is underpinned by two major assumptions; first, the velocity deficit is conserved as the wake linearly expands downstream of the wind turbine, and second, the velocity deficit is only a function of the distance x downstream of the turbine. Accordingly,

$$\delta = \delta(x) = \frac{U_\infty - U(x)}{U_\infty}, \tag{42}$$

where x is the axial distance downwind of the turbine and is often expressed as multiples of the turbine diameter D and $U(x)$ is the wind speed at distance x. In the PARK model, Equation 42 is expressed as,

$$\delta(x) = \frac{2a}{\left(1 + k_w \frac{x}{D}\right)^2}, \tag{43}$$

where k_w is the wake decay coefficient, which is a dimensionless constant and its value depends on the surface roughness. Values of $k_w = 0.04$ and $k_w = 0.078$ are recommended for offshore and onshore conditions respectively. In Eq. (43), the induction factor a is expressed as a function of thrust coefficient C_T as,

$$a = 1 - \sqrt{1 - C_T}. \tag{44}$$

The diameter of the wake D_w is therefore,

$$D_w = D_w(x) = D\left(1 + 2k_w \frac{x}{D}\right). \tag{45}$$

In the PARK model, the only relevant spatial variable is x, and hence, the wind speed and the wind speed deficit along y and z are uniform, which leads to an axis-symmetric conical-shaped wake.

3.6.2 Xie and Archer (XA) model

The XA wake loss model, developed by Xie and Archer [73] is the only wake loss model that truly depends on z and y as it predicts a wake that is not axis-symmetric or conical, but ellipsoidal, which is a more realistic approximation, in particular in the presence of wind shear [74]. The wind speed deficit in the XA model is defined as:

$$\delta = \delta(x, y, z) = \delta_{hub} \exp\left\{-\left[\frac{(z-H)^2}{2\sigma_z^2} + \frac{y^2}{2\sigma_y^2}\right]\right\} \tag{46}$$

$$\delta_{hub} = \delta_{hub}(x) = 1 - \sqrt{1 - \frac{C_T}{8\frac{\sigma_y \sigma_z}{D^2}}} \tag{47}$$

$$\frac{\sigma_y}{D} = \frac{\sigma_y(x)}{D} = k_y \frac{x}{D} + \varepsilon; \quad \frac{\sigma_z}{D} = \frac{\sigma_z(x)}{D} = k_z \frac{x}{D} + \varepsilon, \tag{48}$$

where H is the hub height, $k_y = 0.025$ and $k_z = 0.0175$ are the growth rate of the wake in the y and z directions, obtained from a fit to LES results of a single turbine wake under neutral stability [73].

3.6.3 Bastankah and Porte-Agel (BPA) model

Although the BPA model has an explicit dependency on y and z, where y and z are the span-wise and vertical coordinates, respectively, the cross-section of the wake is always a circle. The wind speed deficit in the BPA model is given by the following equation,

$$\delta = \delta(x, y, z) = \delta_{hub} \exp\left\{-\frac{1}{2\left(k^* \frac{x}{D} + \varepsilon\right)^2}\left[\left(\frac{z-H}{D}\right)^2 + \left(\frac{y}{D}\right)^2\right]\right\} \tag{49}$$

$$\delta_{hub} = \delta_{hub}(x) = 1 - \sqrt{1 - \frac{C_T}{8\left(k^* \frac{x}{D} + \varepsilon\right)^2}} \tag{50}$$

where H is the hub height, $k^* = \frac{\partial \sigma}{\partial x}$ is the growth rate of the wake (which is not the same as $k_w = \frac{\partial D_w}{\partial x}$ in the previous models), σ is the standard deviation of the velocity deficit profile, and $\varepsilon = 0.25\sqrt{\beta}$. In the original study [75], k^* was found to vary between 0.030 and 0.055, from fitting LES results obtained with surface roughness z_0 between 0.5 and 0.00005.

3.6.4 Larsen model

Larsen developed an analytical wake loss model using similarity technique and assuming that the wake region behind a wind turbine can be described via Prandtl's turbulent boundary layer equations [76]. It was also assumed that flow is stationary, incompressible, and the wind shear is negligible. In the Larsen model, which was the recommended model by the European Wind Turbine Standards II (EWTS II) for use in wake loading calculations [77], the wind speed deficit is a function of both axial distance x and radial distance r, while in the PARK model the wake deficit is only a function of axial distance x. In the larsen model, the wind speed deficit is calculated as,

$$\delta = \delta(x, r) = \tag{51}$$

$$-\frac{1}{9}\left[C_T A\left(x + x_0\right)^{-2}\right]^{\frac{1}{3}}\left\{r^{\frac{3}{2}}\left[3c_1^2 C_T A\left(x + x_0\right)\right]^{-\frac{1}{2}} - \left(\frac{35}{2\pi}\right)^{\frac{3}{10}}\left(3c_1^2\right)^{-\frac{1}{5}}\right\}^2,$$

where C_T is the wind turbine thrust coefficient, x and r are the axial and radial distance of the wind turbine of interest from the upstream wind turbine, $A = \pi D^2/4$ is the swept area of the rotor, c_1 is a non-dimensional mixing length defined as,

$$c_1 = \left(\frac{D}{2}\right)^{-\frac{1}{2}}\left(C_T A x_0\right)^{-\frac{5}{6}}, \tag{52}$$

in which x_0 is a non-dimensional reference distance defined as

$$x_0 = \frac{9.5D}{\left(\frac{D_{9.5}}{D}\right)^3} - 1, \tag{53}$$

where is a measure of the wake diameter at distance $9.5D$ given by the following equation,

$$D_{9.5} = D_{nb} + min(H, D_{nb}), \tag{54}$$

where H is hub height and D_{nb} is a corrected wake diameter to take into account the blockage effect of the ground defined as,

$$D_{nb} = max\left[1.08D, 1.08D + 21.7D(I_a - 0.05)\right] \tag{55}$$

where I_a is the ambient turbulence intensity at hub height, assumed to be always greater than 5%. Similar to the PARK model, the wake diameter in the Larsen model is only a function of axial distance x as follows:

$$D_w = D_w(x) = 2\left(\frac{35}{2\pi}\right)^{\frac{1}{5}} \left(3c_1^2\right)^{\frac{1}{5}} \left(C_T A x\right)^{\frac{1}{3}}, \tag{56}$$

Similar to the PARK model, both wake diameter and wind speed deficit in the Larsen model are independent of free stream wind speed U_∞.

3.6.5 Frandsen model

Frandsen et al. [78] developed an analytical wake loss model by applying the momentum equation to a control volume and by assuming self-similarity. They also assumed that the velocity deficit is only a function of the distance x downstream of the turbine and wind speed has a constant profile, similar to that of PARK model. The wind speed deficit in Frandsen model is defined as,

$$\delta = \delta(x) = \frac{1}{2}\left(1 \pm \sqrt{1 - 2\frac{A}{A_w(x)}C_T}\right), \tag{57}$$

in which A is the swept area of the rotor and $A_w(x) = \pi D_w^2(x)/4$ is the cross section of the wake area at distance x downstream of the turbine, where $D_w(x)$ is the wake diameter and is defined as,

$$D_w(x) = D\left(\beta^{\frac{k}{2}} + \alpha\frac{x}{D}\right)^{\frac{1}{k}}, \tag{58}$$

in which $\alpha = 0.7$, k is either 3 (Schlichting solution) or 2 (square root shape solution) [79], and β is the wake expansion parameter and is defined as,

$$\beta = \frac{1+\sqrt{1-C_T}}{2\sqrt{1-C_T}}. \tag{59}$$

It should be mentioned that the Frandsen model is recommended for both small and large regular wind farms with rectangular shapes and equal spacings between turbines. Similar to the PARK and Larsen models, the Frandsen model is also independent of free stream velocity U_∞.

3.6.6 Geometric model (GM)

The geometric model (GM) is a hybrid wake loss model that estimates the relative power generated by any downstream turbine with respect to the power generated by the front-row turbine [80]. The GM is considered as a hybrid model because it does not simulate the physical processes occurring in wakes, but rather uses empirical coefficients, derived from a multi-linear regression, to relate relative power production of a wind turbine sited in a wind farm to its geometric quantities, namely blockage ratio BR and blockage distance BD.

The blockage ratio BR_i of a wind turbine i in a given wind direction is the fraction of the swept area of turbine i that is blocked by the swept area of any upstream turbine. Value of BR is always between 0 and 1. A blockage ratio of 0 in a given wind direction means that the turbine is not blocked at all and receives undisturbed wind in that direction, whereas a blockage ratio of 1 means that the turbine is completely blocked by the upstream wind turbines.

The blockage distance BD_i of wind turbine i, however, is a measure of the distance between the wind turbine of interest and the upstream blocking turbines. Hence, a larger blockage distance means a greater wind speed recovery, lower wake losses, and consequently more power production. Blockage ratio and blockage distance of a wind turbine for a given wind direction are calculated using the following equations:

$$BR_i = \frac{1}{A} \int_A \chi dA, \tag{60}$$

$$BD_i = \frac{1}{A} \int_A L\chi dA, \tag{61}$$

where $\chi = 1$ wherever the swept area of turbine i is blocked and zero otherwise, and L denotes the distance to the upstream blocking turbine. Once the two geometric properties are calculated for a given wind direction, then the relative power is obtained as follows:

$$P_i^{REL} = \frac{P_i}{P_{front}} = \begin{cases} \alpha + \beta BR_i + \gamma BD_i/L_\infty & BR_i \neq 0, \\ 1 & BR_i = 0, \end{cases} \tag{62}$$

where P_i and P_{front} are the power generated by turbine i and by the front turbine, and the fitting coefficients α, β, and γ depend on atmospheric stability. In the original paper [80], only values for neutral stability are presented.

3.6.7 Wake overlapping

When multiple wakes overlap, like in a wind farm, the wake overlapping is simply performed by taking the square root of the sum of the squared wind speed deficits induced by each individual wind turbine [72]. Hence, the total wind speed deficit at the location of turbine

j is,

$$\delta_{TOT} = \sqrt{\sum_{n=1}^{N} \delta_i^2(x_{ij})}, \tag{63}$$

where N is the number of upstream wind turbines and x_{ij} is the distance between turbine j and the upstream turbine i. Depending on the employed model, each $\delta_i(x_{ij})$ is calcultated using one of the wind speed deficit equations, i.e., either Eq. (43), or Eq. (46), or Eq. (49), or Eq. (51), or Eq. (57). Substituting the total wind speed deficit δ_{TOT} in $U_j = (1-\delta_{TOT})U_\infty$ yields the wind speed experience by the wind turbine of interest U_j, and since wind power density is proportional to the cube of wind speed, relative power of turbine j is calculated as,

$$P_{rel,j} = \left(\frac{U_j}{U_\infty}\right)^3 \tag{64}$$

where $P_{rel,j}$ is a measure of power produced by wind turbine j divided by the maximum power that is produced at the front row. The sum of squares (SS) method described in this section is the most popular wake overlapping technique used in industry. In addition to the SS technique, three other approaches have been introduced in literature, including the geometric superposition, the linear superposition, and the sum of energy deficits [81].

4 Search algorithms

A list of most popular search algorithms used for wind farm layout optimization analyses are presented in Table 4. According to literature, Genetic Algorithm (hereafter GA) is the most popular search algorithm that has been used to perform wind farm layout optimization analysis. The general procedure of the GA is illustrated in Fig. 3. First, the search process is *initialized* by creating random strings of 1 and 0, respectively standing for places with turbine

Table 4: Popular search algorithms for wind farm layout optimization problem.

Optimization technique	Studies
Genetic Algorithms	[50, 18, 57, 82, 7, 49]
	[12, 83, 84, 56, 85, 86, 36]
Greedy Algorithms	[5, 9, 87, 88, 40]
Particle Swarm Optimization	[18, 85, 17, 89, 90, 20, 52, 91]
Ant Colony Search Algorithm	[92, 93, 94]
Mixed Integer Linear and Quadratic Optimization	[95, 96, 97, 19, 98]
Spread Sheet	[99]
Simulated Annealing	[54, 100, 40]
Definite Point Selection	[101]

and without turbines. Then, the *selection*, which is to select and retain certain layouts that can generate higher annual energy productions according to a given selection probability, is conducted. During the *crossover*, selected layouts (parents) are combined to create new layouts (children). Then, parts of the layouts are randomly changed during the *mutation*. In the last step, layouts of the initial population are *replaced* with new layouts (children) that have been generated provided that the new layouts perform better in comparison with the layouts of the initial population. This process continues until the solutions converges or the termination criteria are met.

A Greedy Algorithm is a heuristic procedure that tries to find an optimal solution close to the global optimum by determining a locally optimal solution at each stage. For instance, one wind turbine is randomly located within the legal area of the wind farm, and then the location of the second turbine is determined so that the annual energy production of the combination of the two turbines is optimized. Then, the optimal location of the third turbine is determined so that the annual energy production of the combination of the three turbines is maximized. This process continues until all turbines are placed within the wind farm area.

Particle Swarm Optimization (hereafter PSO), developed by Kennedy and Eberhart [102], is a population based stochastic optimization technique that iteratively improves a candidate solution. The PSO technique is somehow similar to the Genetic Algorithm as the procedure is initialized using a population of random solutions. The major difference between the PSO

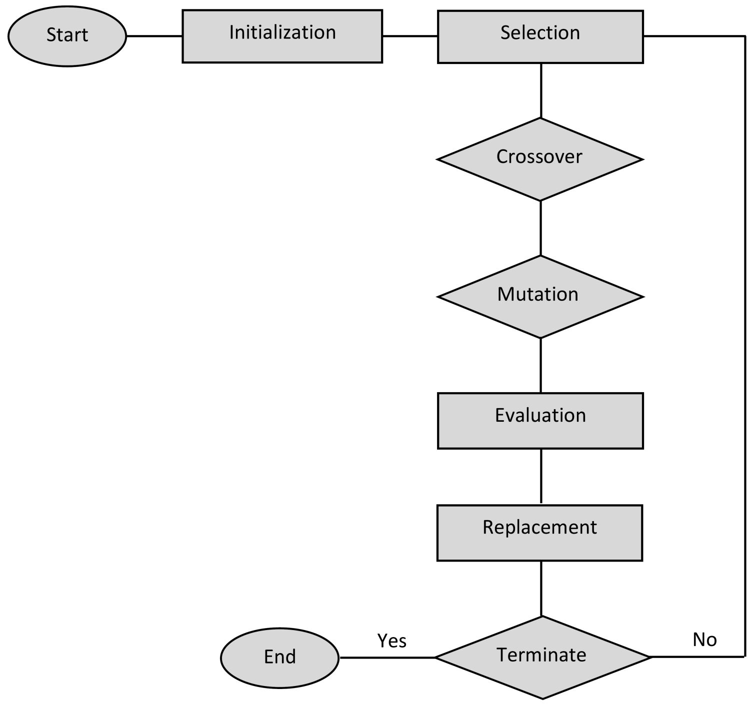

Figure 3: Genetic algorithm.

and the Genetic Algorithm is that in the PSO a randomized velocity is also assigned to each potential solution based on which the potential solutions, which are called particles, evolve through the hyperspace.

In nature, ants initially move around randomly when they are searching for food, and once they find a food source they leave a pheromone trail on the ground on their way transferring the food back to their colony. This pheromone trail helps other ants to not to move on random paths, but instead to follow the trail to the food source. Based on this behavior, Marco Dorigo [103] developed an optimization algorithm namely Ant Colony Search Algorithm (hereafter ACSA). The ACSA has been adapted for the wind farm layout optimization problem by several researchers of this field. For instance, Eroğlu and Seçkiner [93] developed an algorithm in which the contribution of each turbine to the total wake losses of the farm is assumed to be the pheromone. Accordingly, more ants are assigned to turbines with higher pheromone to improve their location. Ants move these turbines in random locations, and if any new location causes the total annual energy production of the wind farm to increase, then the previous layout will be replaced by the newly found more efficient layout. This procedure continues until a convergence occurs.

Simulated Annealing (hereafter SA) is a probabilistic optimization technique which is more applicable to discrete spaces where determining an approximate global optimum is more preferred than a precise local optimum over the same amount of time. In fact, the SA is an approach that attempts to avoid entrapment in a poor local maximum by allowing an occasional downhill move. The acceptance of a downhill move depends on a control parameter, called the temperature, and on the magnitude of the variation. Rivas et al. (2009) used the SA algorithm coupled with a local search module to preform a wind farm layout optimization analysis. The disadvantage of the employed local search was its likelihood of finding a local rather than a global optimum. The main idea behind the SA algorithm developed by Rivas et al. (2009) is that the algorithm moves to a neighboring layout by removing a turbine, adding a turbine, or moving a turbine, and then, the annual energy production is calculated for the new layout. If the annual energy production of the new layout has increased in comparison to the previous layout, the new layout may be readily accepted, however, if the annual energy production has decreased, the new layout is accepted according to the probability calculated via the following equation,

$$P(\delta AEP) = exp(-|\delta AEP|/t) \tag{65}$$

where δAEP is the variation of the annual energy production from the previous layout to the new layout and t stands for the control parameter called temperature that is gradually cooled (decreased) to make the system converge.

In the Definite Point Selection algorithm (hereafter DPS), developed by Shakoor et al. [101], the wake of each wind turbine is assumed to be a triangle with one vertex located upstream of the turbine and the other two vertices located downwind of the turbine (see Fig. 4a). The divergence angle of the wake triangle is calculated as $\gamma = 2tan^{-1}(\alpha)$ where α is the entrainment constant and is defined as $\alpha = 0.5/ln(z/z_0)$ in which z and z_0 are turbine hub height and surface roughness respectively. Overlapping of the wake triangles associated with wind turbines of a wind farm forms a wake polygon with n vertices (see Fig. 4b). The shape and the area of this polygon varies with the wind direction, hence, there are A_i polygons where $i = 1 : 360$ stands for the wind direction. A point inside the wind farm area that does not fall inside any of the predetermined wake polygons is then selected as the best position for placing the next turbine inside the wind farm area.

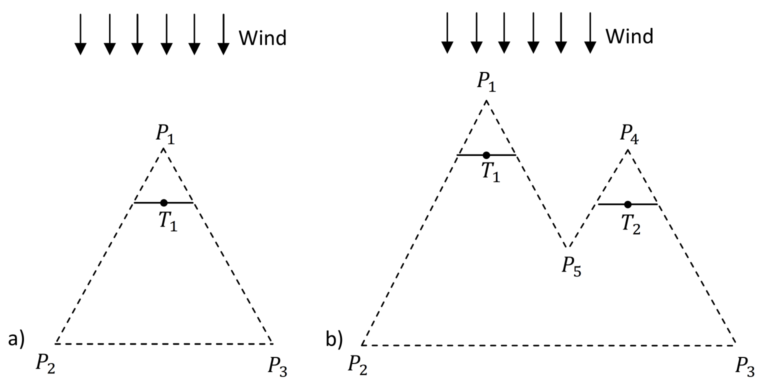

Figure 4: (a) Wake triangle and (b) wake polygon employed in Definite Point Selection algorithm to select the optimal place for wind turbines.

5 Practice your knowledge

Increasing climate change concerns and extremely high economic, health and social expenses caused by adverse environmental impacts of fossil fuels have pushed the energy industry towards sustainable energy resources, in particular, wind energy. Although wind energy provides approximately 8% of the United States generating capacity [104], which is more than any other renewable source, the global contribution of wind energy is yet too small and for wind energy to play a more significant role in the market the issues associated with the wind farm under-performance must be addressed. Solving the wind farm layout optimization problem is the most demanding task of wind farm design and development, hence, considerable research is actively conducted to develop more efficient solutions to this problem. Latest findings, references and investigations on the major concepts associated with the wind farm layout optimization problem were reviewed and discussed in this chapter. That includes objective functions, optimization variables, wake loss models, and search algorithms. In this section, some specific cases are proposed to assist the readers to put the knowledge shared in this chapter into practice to some extent.

Case I: Shape of the wind farm

If the area of the two lands given in Figure 5a are equal ($A_1 = A_2$), and assuming that the wind frequency at the location of both sites is as presented in Figure 5b, explain which area is more suitable for developing a wind farm.

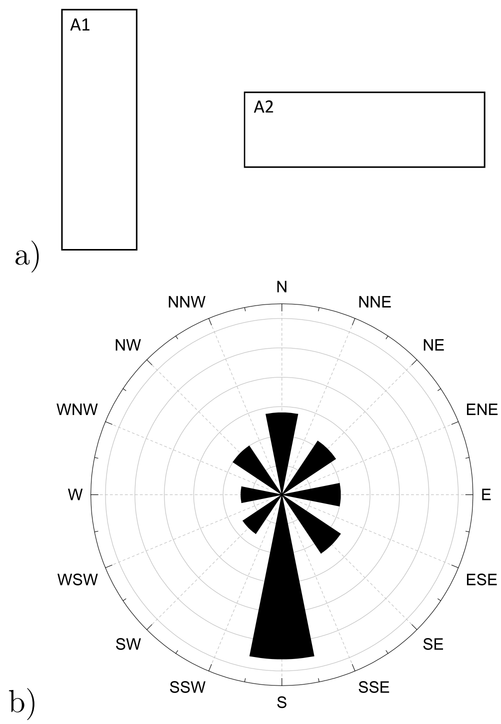

Figure 5: Case I.

Case II: Wake of wind turbines

A square land is available for developing a wind farm with 5 horizontal axis wind turbines (see Figure 6). If wind frequency at the location of this land is as presented in Figure 6a, explain which of the three layouts proposed in Figures 6b to 6d is likely to be the most efficient one.

Case III: Wind speed deficit in wind farms

The layout of the Lillgrund wind farm, an offshore wind farm in Sweden with 48 SWT-

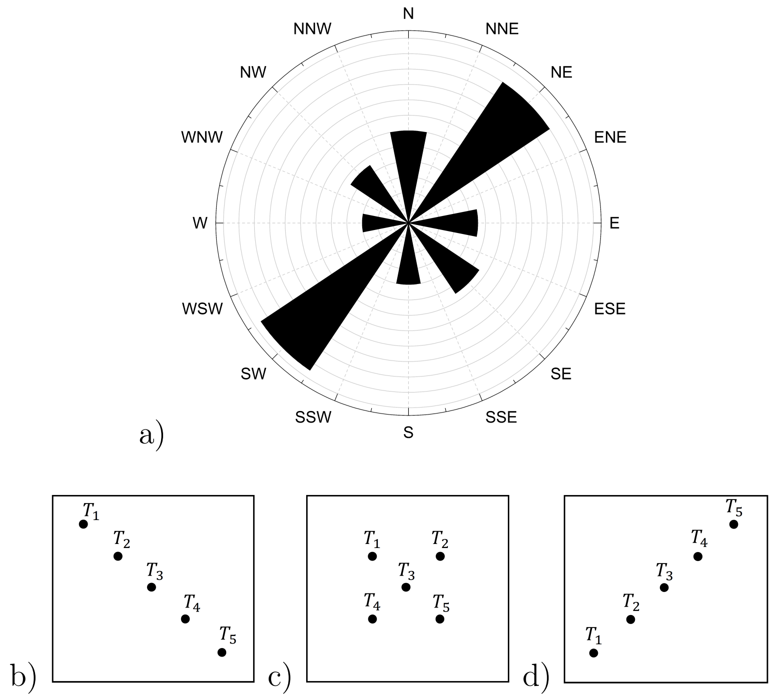

Figure 6: Case II.

2.3-93 wind turbines, is given in Figure 7. Assuming a southwesterly wind scenario along the direction of alignment of the wind turbines, draw a qualitative plot that illustrates the variation of the relative power production of wind turbines along columns C_1 and C_2. (Hint: Relative power production of a wind turbine at a given wind direction is defined as the ratio of power produced by that wind turbine to the power produced by the front row turbine. Hence, the relative power production of front row turbines is always 1, while the relative power productions of all downwind turbines are below 1.)

Case IV: Yaw angle of wind turbines

Norrekaer is an onshore wind farm with 13 Siemens SWT 2.3-93 wind turbines. The layout of this wind farm is illustrated in Figure 8. First, draw a qualitative plot that shows the variation of the relative power production of wind turbines along the column. How does this plot change if turbine 5 is yawed by 20 degrees as is illustrated in Figure 8b. How would

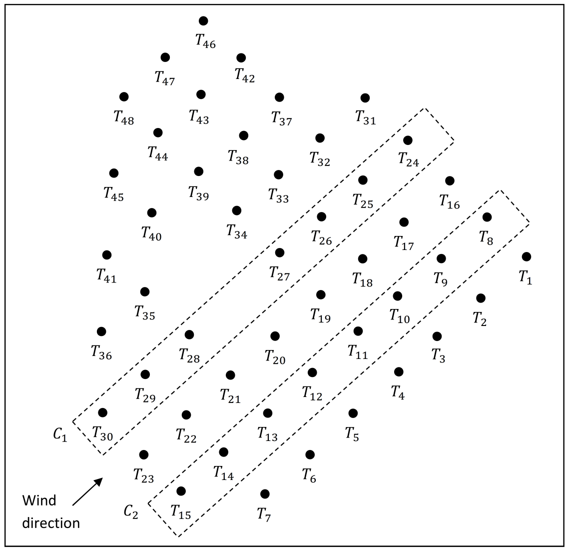

Figure 7: Cases III and XI.

the plot change if turbine 5 was yawed in the opposite direction?

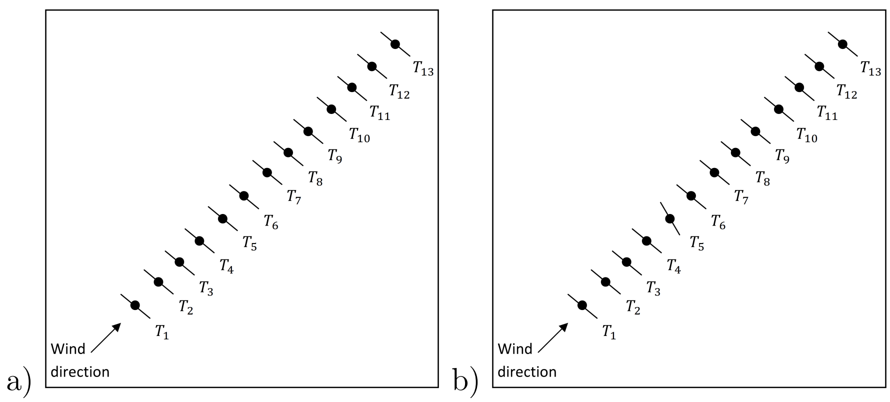

Figure 8: Problems IV and V.

Case V: Variation of power production with wind direction

Plot the relative power production of turbine T22 in Figure 7 and turbine T2 in Figure 8a versus wind direction for wind directions varying from 0° to 360° with respect to the North.

Case VI: Surface roughness

How does the surface roughness affect the performance of a wind farm? Explain using the logarithmic boundary layer profile. A community wind farm and its associated wind rose is presented in Figure 9. Which turbine has the lowest production and needs to be relocated? Which turbine has the highest production?

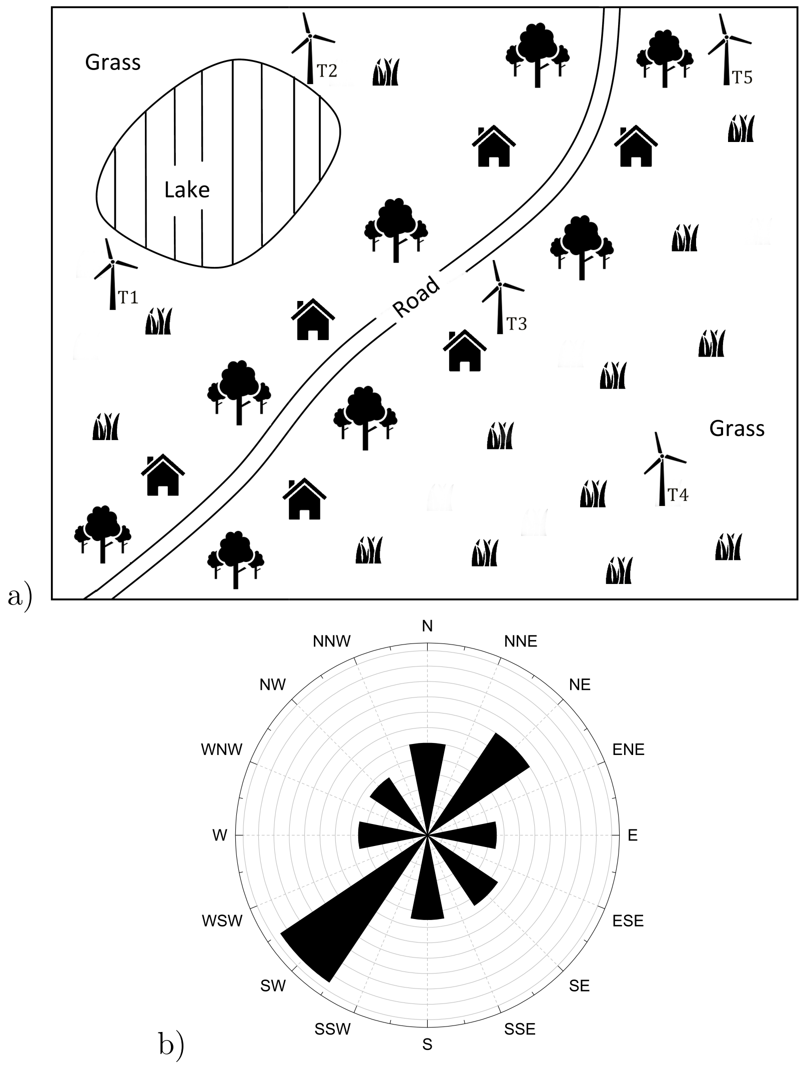

Figure 9: Case VI.

Case VII: Inner turbines versus outer turbines

Figure 10a illustrates the wind frequency at the location of the area given in Figure 10b.

Among layouts proposed in Figures 10c and 10d, which one is potentially a more efficient one?

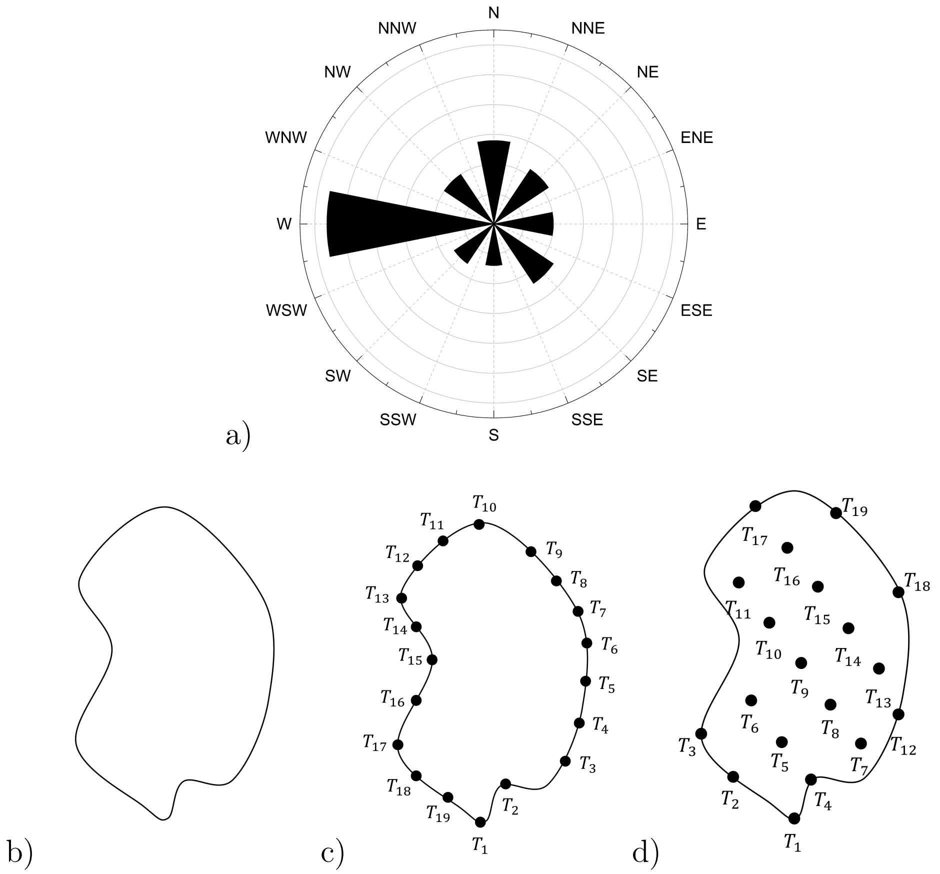

Figure 10: Case VII.

Case VIII: Wind farm noise production

In Figure 11, coordinates of the house and four SWT-2.3-96 wind turbines are (1337,292), (279,215), (395,821), (757,1243), and (1337,1431) m, respectively. Assuming that the wind turbines are the only noise sources, estimate the total sound pressure level at the location of the house.

Case IX: Hub height optimization

Assume both turbines shown in Figure 2 are SWT-2.3-93 manufactured by Siemens com-

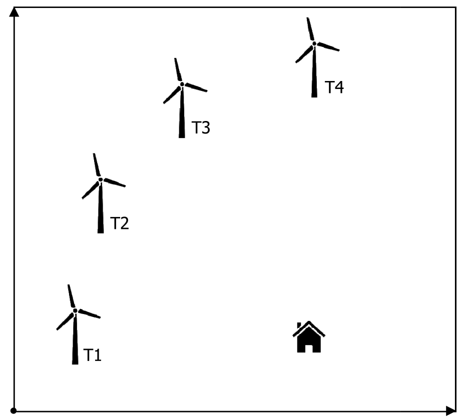

Figure 11: Case VIII.

pany. If $H_u = H_{max} = 120\ m$, then plot the relative power of the downwind turbine versus its hub height H_d, where $10\ m \leq H_d \leq H_{max}$.

Case X: Fatigue loads

How does the thrust coefficient of a wind turbine relate to the fatigue loads acting on that turbine?

Case XI: Turbine type

How would the annual energy production of the Lillgrund wind farm change if turbines T_i, where $i = 2$, 4, 6, 8, 9, 10, 11, 12, 13, 14, 15, 24, 25, 26, 27, 28, 29, 30, 32, 34, 35, 37, 38, 39, 40, 41, 42, 44, 46, 47, 48, were removed and the rest of them were replaced by SWT-8.0-154 turbines (see Figure 7). Conduct your calculations using the PARK model described in section 3.6.1 and the wind rose given in Vasel-Be-Hagh and Archer [5].

Case XII: Atmospheric stability

Atmospheric stability is a term used to qualitatively describe the potential for vertical motion in the atmosphere. Atmosphere is considered stable when it is stratified without any vertical motion. This condition usually exists at night time, when there is a negative heat flux at the surface and the air is cooled down from the bottom. On the other hand, when the air is heated up from the bottom, which usually happens during day time, strong vertical motions are generated and atmosphere is considered unstable. At sunset and sunrise, when the heat flux from the surface is approximately zero, atmosphere is considered neutral. Explain the effect of atmospheric stability on the wake of wind turbines and power production of wind farms assuming an equal geostrophic wind speed.

Case XIII: Wind farms and hurricanes

Discuss the possibility of using wind turbines to protect communities against hurricanes (see [105]).

References

[1] Prateek Mittal, Kishalay Mitra, and Kedar Kulkarni. Optimizing the number and locations of turbines in a wind farm addressing energy-noise trade-off: A hybrid approach. *Energy Conversion and Management*, 132:147 – 160, 2017.

[2] L. Chen, C. Harding, A. Sharma, and E. MacDonald. Modeling noise and lease soft costs improves wind farm design and cost-of-energy predictions. *Renewable Energy*, 97:849–859, 2016.

[3] Bryony DuPont, Jonathan Cagan, and Patrick Moriarty. An advanced modeling system for optimization of wind farm layout and wind turbine sizing using a multi-level extended pattern search algorithm. *Energy*, 106:802 – 814, 2016.

[4] O. Rahbari, M. Vafaeipour, F. Fazelpour, M. Feidt, and M.A. Rosen. Towards realistic designs of wind farm layouts: Application of a novel placement selector approach. *Energy Conversion and Management*, 81:242–254, 2014.

[5] A.R. Vasel-Be-Hagh and C.L. Archer. Wind farm hub height optimization. *Applied Energy*, forthcoming(195):905–921, 2017.

[6] S.A. MirHassani and A. Yarahmadi. Wind farm layout optimization under uncertainty. *Renewable Energy*, 107:288–297, 2017.

[7] Ying Chen, Hua Li, Kai Jin, and Yousri Elkassabgi. Investigating the possibility of using different hub height wind turbines in a wind farm. *International Journal of Sustainable Energy*, 36(2):142–150, 2017.

[8] Longyan Wang, Andy C.C. Tan, Michael Cholette, and Yuantong Gu. Comparison of the effectiveness of analytical wake models for wind farm with constant and variable hub heights. *Energy Conversion and Management*, 124:189 – 202, 2016.

[9] K. Chen, M.X. Song, X. Zhang, and S.F. Wang. Wind turbine layout optimization with multiple hub height wind turbines using greedy algorithm. *Renewable Energy*, 96:676 – 686, 2016.

[10] Ying Chen, Hua Li, Kai Jin, and Qing Song. Wind farm layout optimization using genetic algorithm with different hub height wind turbines. *Energy Conversion and Management*, 70:56 – 65, 2013.

[11] A.R. Vasel-Be-Hagh and C.L. Archer. Wind farms with counter-rotating wind turbines. *Sustainable Energy Technologies and Assessments*, 2016.

[12] A.C. Pillai, J. Chick, L. Johanning, M. Khorasanchi, and S. Pelissier. Optimisation of offshore wind farms using a genetic algorithm. *International Journal of Offshore and Polar Engineering*, 26(3):225–234, 2016.

[13] J. Feng, W.Z. Shen, and C. Xu. Multi-objective random search algorithm for simultaneously optimizing wind farm layout and number of turbines. *Journal of Physics: Conference Series*, 753(3), 2016.

[14] P.-E. Réthoré, P. Fuglsang, G.C. Larsen, T. Buhl, T.J. Larsen, and H.A. Madsen. Topfarm: Multi-fidelity optimization of wind farms. *Wind Energy*, 17(12):1797–1816, 2014.

[15] B. Van Eeckhout, D. Van Hertem, M. Reza, K. Srivastava, and R. Belmans. Economic comparison of vsc hvdc and hvac as transmission system for a 300mw offshore wind farm. *European Transactions on Electrical Power*, 20(5):661–671, 2010.

[16] R.J.A.M. Stevens, B.F. Hobbs, A. Ramos, and C. Meneveau. Combining economic and fluid dynamic models to determine the optimal spacing in very large wind farms. *Wind Energy*, 20(3):465–477, 2017.

[17] P. Hou, W. Hu, M. Soltani, C. Chen, and Z. Chen. Combined optimization for offshore wind turbine micro siting. *Applied Energy*, 189:271–282, 2017.

[18] L. Amaral and R. Castro. Offshore wind farm layout optimization regarding wake effects and electrical losses. *Engineering Applications of Artificial Intelligence*, 60:26–34, 2017.

[19] A. Wędzik, T. Siewierski, and M. Szypowski. A new method for simultaneous optimizing of wind farm's network layout and cable cross-sections by milp optimization. *Applied Energy*, 182:525–538, 2016.

[20] P. Hou, W. Hu, and Z. Chen. Optimisation for offshore wind farm cable connection layout using adaptive particle swarm optimisation minimum spanning tree method. *IET Renewable Power Generation*, 10(5):694–702, 2016.

[21] N.S. Ghaisas and C.L. Archer. Geometry-based models for studying the effects of wind farm layout. *Journal of Atmospheric and Oceanic Technology*, 33(3):481–501, 2016.

[22] A.G. Gonzalez-Rodriguez, M. Burgos-Payan, J. Riquelme-Santos, and J. Serrano-Gonzalez. Reducing computational effort in the calculation of annual energy produced in wind farms. *Renewable and Sustainable Energy Reviews*, 43:656–665, 2015.

[23] M.T. van Dijk, J.-W. van Wingerden, T. Ashuri, and Y. Li. Wind farm multi-objective wake redirection for optimizing power production and loads. *Energy*, 121:561–569, 2017.

[24] M.T. Van Dijk, J.-W. Van Wingerden, T. Ashuri, Y. Li, and M.A. Rotea. Yaw-misalignment and its impact on wind turbine loads and wind farm power output. *Journal of Physics: Conference Series*, 753(6), 2016.

[25] J. Park and K.H. Law. Bayesian ascent: A data-driven optimization scheme for real-time control with application to wind farm power maximization. *IEEE Transactions on Control Systems Technology*, 24(5):1655–1668, 2016.

[26] J. Park and K.H. Law. Cooperative wind turbine control for maximizing wind farm power using sequential convex programming. *Energy Conversion and Management*, 101:295–316, 2015.

[27] M. Abdulrahman and D. Wood. Some effects of efficiency on wind turbine interference and maximum power production. *Wind Engineering*, 39(5):495–506, 2015.

[28] M. Song, K. Chen, X. Zhang, and J. Wang. Optimization of wind turbine micro-siting for reducing the sensitivity of power generation to wind direction. *Renewable Energy*, 85:57–65, 2016.

[29] L. Wang, A.C.C. Tan, M.E. Cholette, and Y. Gu. Optimization of wind farm layout with complex land divisions. *Renewable Energy*, 105:30–40, 2017.

[30] A. Rabiee and S.M. Mohseni-Bonab. Maximizing hosting capacity of renewable energy sources in distribution networks: A multi-objective and scenario-based approach. *Energy*, 120:417–430, 2017.

[31] X. Gao, H. Yang, and L. Lu. Study on offshore wind power potential and wind farm optimization in hong kong. *Applied Energy*, 130:519–531, 2014.

[32] S. Chowdhury, J. Zhang, A. Messac, and L. Castillo. Optimizing the arrangement and the selection of turbines for wind farms subject to varying wind conditions. *Renewable Energy*, 52:273–282, 2013.

[33] P. Hou, W. Hu, B. Zhang, M. Soltani, C. Chen, and Z. Chen. Optimised power dispatch

strategy for offshore wind farms. *IET Renewable Power Generation*, 10(3):399–409, 2016.

[34] T. Ashuri, C. Ponnurangam, J. Zhang, and M. Rotea. Integrated layout and support structure optimization for offshore wind farm design. *Journal of Physics: Conference Series*, 753(9), 2016.

[35] S. Pookpunt and W. Ongsakul. Design of optimal wind farm configuration using a binary particle swarm optimization at huasai district, southern thailand. *Energy Conversion and Management*, 108:160–180, 2016.

[36] X. Gao, H. Yang, and L. Lu. Investigation into the optimal wind turbine layout patterns for a hong kong offshore wind farm. *Energy*, 73:430–442, 2014.

[37] Le Chen and Erin MacDonald. A system-level cost-of-energy wind farm layout optimization with landowner modeling. *Energy Conversion and Management*, 77:484 – 494, 2014.

[38] T. Ashuri, M.B. Zaaijer, J.R.R.A. Martins, G.J.W. van Bussel, and G.A.M. van Kuik. Multidisciplinary design optimization of offshore wind turbines for minimum levelized cost of energy. *Renewable Energy*, 68:893–905, 2014.

[39] M. Rezaei Mirghaed and R. Roshandel. Site specific optimization of wind turbines energy cost: Iterative approach. *Energy Conversion and Management*, 73:167–175, 2013. cited By 21.

[40] C.N. Elkinton, J.F. Manwell, and J.G. McGowan. Algorithms for offshore wind farm layout optimization. *Wind Engineering*, 32(1):67–83, 2008.

[41] M.A. Lackner and C.N. Elkinton. An analytical framework for offshore wind farm layout optimization. *Wind Engineering*, 31(1):17–31, 2007.

[42] W. Li, E. Özcan, and R. John. Multi-objective evolutionary algorithms and hyper-heuristics for wind farm layout optimisation. *Renewable Energy*, 105:473–482, 2017.

[43] S. Chowdhury, A. Mehmani, J. Zhang, and A. Messac. Market suitability and performance tradeoffs offered by commercialwind turbines across differingwind regimes. *Energies*, 9(5), 2016.

[44] S. Shamshirband, D. Petković, Ž. Ćojbašić, V. Nikolić, N.B. Anuar, N.L. Mohd Shuib, M.L. Mat Kiah, and S. Akib. Adaptive neuro-fuzzy optimization of wind farm project net profit. *Energy Conversion and Management*, 80:229–237, 2014.

[45] W.Y. Kwong, P.Y. Zhang, D. Romero, J. Moran, M. Morgenroth, and C. Amon. Multi-objective wind farm layout optimization considering energy generation and noise propagation with nsga-ii. *Journal of Mechanical Design, Transactions of the ASME*, 136(9), 2014.

[46] S. Yamani Douzi Sorkhabi, D.A. Romero, G.K. Yan, M.D. Gu, J. Moran, M. Morgenroth, and C.H. Amon. The impact of land use constraints in multi-objective energy-noise wind farm layout optimization. *Renewable Energy*, 85:359–370, 2016.

[47] S.S. Rodrigues and A.C. Marta. On addressing noise constraints in the design of wind turbine blades. *Structural and Multidisciplinary Optimization*, 50(3):489–503, 2014.

[48] E. Muljadi and C.P. Butterfield. Pitch-controlled variable-speed wind turbine generation. *IAS Annual Meeting (IEEE Industry Applications Society)*, pages 323–330, 1999.

[49] D. Guirguis, D.A. Romero, and C.H. Amon. Toward efficient optimization of wind farm layouts: Utilizing exact gradient information. *Applied Energy*, 179:110–123, 2016.

[50] L. Parada, C. Herrera, P. Flores, and V. Parada. Wind farm layout optimization using a gaussian-based wake model. *Renewable Energy*, 107:531–541, 2017.

[51] J.Y.J. Kuo, D.A. Romero, J.C. Beck, and C.H. Amon. Wind farm layout optimization on complex terrains – integrating a cfd wake model with mixed-integer programming. *Applied Energy*, 178:404–414, 2016.

[52] H. Yang, K. Xie, H.-M. Tai, and Y. Chai. Wind farm layout optimization and its application to power system reliability analysis. *IEEE Transactions on Power Systems*, 31(3):2135–2143, 2016.

[53] N. Quan and H.M. Kim. A mixed integer linear programing formulation for unrestricted wind farm layout optimization. *Journal of Mechanical Design, Transactions of the ASME*, 138(6), 2016.

[54] E.A. Hernandez, V. Uddameri, and S. Singaraju. Combined optimization of a wind farm and a well field for wind-enabled groundwater production. *Environmental Earth Sciences*, 71(6):2687–2699, 2014.

[55] J.C. Bansal and P. Farswan. Wind farm layout using biogeography based optimization. *Renewable Energy*, 107:386–402, 2017. cited By 0.

[56] Y. Chen, H. Li, B. He, P. Wang, and K. Jin. Multi-objective genetic algorithm based innovative wind farm layout optimization method. *Energy Conversion and Management*, 105:1318–1327, 2015.

[57] M. Abdulrahman and D. Wood. Investigating the power-coe trade-off for wind farm layout optimization considering commercial turbine selection and hub height variation. *Renewable Energy*, 102:267–278, 2017.

[58] S. Chowdhury, J. Zhang, W. Tong, and A. Messac. Modeling the influence of land-shape on the energy production potential of a wind farm site. *Journal of Energy Resources Technology, Transactions of the ASME*, 136(1), 2014.

[59] W. Tong, S. Chowdhuryt, and A. Messac. A consolidated visualization of wind farm energy production potential and optimal land shapes under different land area and nameplate capacity decisions. 2014.

[60] L. Wang, A.C.C. Tan, Y. Gu, and J. Yuan. A new constraint handling method for wind farm layout optimization with lands owned by different owners. *Renewable Energy*, 83:151–161, 2015.

[61] J. Smagorinsky. General circulation experiments with the primitive equations. *Monthly Weather Review*, 91(3):99–164, 1963.

[62] Chin-Hoh Moeng. A large eddy simulation model for the study of planetary boundary-layer turbulence. *Journal of the Atmospheric Sciences*, 41(13):2052–2062, 1984.

[63] J.N. Sørensen and W.Z. Shen. Numerical modeling of wind turbine wakes. *Journal of Fluids Engineering, Transactions of the ASME*, 124(2):393–399, 2002.

[64] Luis A. Martinez-Tossas, Matthew J. Churchfield, and Stefano Leonardi. Large eddy simulations of the flow past wind turbines: actuator line and disk modeling. *Wind Energy*, 18(6):1047–1060, 2015.

[65] P. Doubrawa, R.J. Barthelmie, H. Wang, and M.J. Churchfield. A stochastic wind turbine wake model based on new metrics for wake characterization. *Wind Energy*, 20(3):449–463, 2017.

[66] D. Bastine, L. Vollmer, M. Wächter, and J. Peinke. Stochastic wake modeling based on pod analysis. *Wind Energy Science Discussions*, 2016:1–36, 2016.

[67] N. Ali, H.F. Kadum, and R.B. Cal. Focused-based multifractal analysis of the wake in a wind turbine array utilizing proper orthogonal decomposition. *Journal of Renewable and Sustainable Energy*, 8(6), 2016.

[68] J.F. Ainslie. Calculating the flowfield in the wake of wind turbines, 1988.

[69] S. Ott, J. Berg, and M. Nielsen. Linearised cfd models for wakes. Technical report, Danmarks Tekniske Universitet, RisøNationallaboratoriet for Bæredygtig Energi, 2011.

[70] T. Ishihara, A. Yamaguchi, and Y. Fujino. Developmentof a new wake model based on a wind tunnel experiment. Technical report, Global Wind, 2004.

[71] Niels Otto Jensen. A note on wind generator interaction. Tech. Note Risø-M-2411, Risø National Laboratory, Denmark, 1983.

[72] I Katic, J Højstrup, and Niels Otto Jensen. A simple model for cluster efficiency. In *European Wind Energy Association Conference and Exhibition*, pages 407–410, 1986.

[73] Shengbai Xie and Cristina Archer. Self-similarity and turbulence characteristics of wind turbine wakes via large-eddy simulation. *Wind Energy*, 18(10):1815–1838, 2015.

[74] S. Xie, C.L. Archer, N. Ghaisas, and C. Meneveau. Benefits of collocating vertical-axis and horizontal-axis wind turbines in large wind farms. *Wind Energy*, 20(1):45–62, 2017.

[75] M. Bastankhah and F. Porté-Agel. A new analytical model for wind-turbine wakes. *Renewable Energy*, 70:116–123, 2014.

[76] Gunner C Larsen. A simple wake calculation procedure. Tech. Note Risø-M-2760, Risø National Laboratory, Denmark, 1988.

[77] J.T.G. Pierik, J.W.M. Dekker, H. Braam, B.H. Bulder, D. Winkelaar, Gunner Chr. Larsen, E. Morfiadakis, P. Chaviaropoulos, A. Derrick, and J.P. Molly. *European wind turbine standards II (EWTS-II)*, pages 568–571. James and James Science Publishers, 1999.

[78] Sten Frandsen, Rebecca Barthelmie, Sara Pryor, Ole Rathmann, Søren Larsen, Jørgen Højstrup, and Morten Thøgersen. Analytical modelling of wind speed deficit in large offshore wind farms. *Wind Energy*, 9(1-2):39–53, 2006.

[79] RJ Barthelmie, GC Larsen, ST Frandsen, L Folkerts, K Rados, SC Pryor, B Lange, and G Schepers. Comparison of wake model simulations with offshore wind turbine wake profiles measured by sodar. *Journal of Atmospheric and Oceanic Technology*, 23(7):888–901, 2006.

[80] Niranjan Ghaisas and Cristina L Archer. Geometry-based models for studying the effect of wind farm layout. *Journal of Atmospheric and Oceanic Technology*, 23(3):481–501, 2016.

[81] J.Y.J. Kuo, D.A. Romero, and C.H. Amon. A mechanistic semi-empirical wake interaction model for wind farm layout optimization. *Energy*, 93:2157–2165, 2015.

[82] Y.-H. Zhang, Y.-J. Gong, T.-L. Gu, Y. Li, and J. Zhang. Flexible genetic algorithm: A simple and generic approach to node placement problems. *Applied Soft Computing Journal*, 52:457–470, 2017.

[83] B. DuPont and J. Cagan. A hybrid extended pattern search/genetic algorithm for multi-stage wind farm optimization. *Optimization and Engineering*, 17(1):77–103, 2016.

[84] P. Mittal, K. Kulkarni, and K. Mitra. A novel hybrid optimization methodology to

optimize the total number and placement of wind turbines. *Renewable Energy*, 86:133–147, 2016.

[85] H. Long and Z. Zhang. A two-echelon wind farm layout planning model. *IEEE Transactions on Sustainable Energy*, 6(3):863–871, 2015.

[86] J. Feng and W.Z. Shen. Solving the wind farm layout optimization problem using random search algorithm. *Renewable Energy*, 78:182–192, 2015.

[87] K. Chen, M.X. Song, and X. Zhang. The iteration method for tower height matching in wind farm design. *Journal of Wind Engineering and Industrial Aerodynamics*, 132:37–48, 2014.

[88] K. Chen, M.X. Song, and X. Zhang. The investigation of tower height matching optimization for wind turbine positioning in the wind farm. *Journal of Wind Engineering and Industrial Aerodynamics*, 114:83–95, 2013.

[89] B. Zhang, B. Song, Z. Mao, and W. Tian. A novel wake energy reuse method to optimize the layout for savonius-type vertical axis wind turbines. *Energy*, 121:341–355, 2017.

[90] P. Hou, W. Hu, C. Chen, M. Soltani, and Z. Chen. Optimization of offshore wind farm layout in restricted zones. *Energy*, 113:487–496, 2016.

[91] W. Tong, S. Chowdhury, and A. Messac. A multi-objective mixed-discrete particle swarm optimization with multi-domain diversity preservation. *Structural and Multidisciplinary Optimization*, 53(3):471–488, 2016.

[92] Y.-K. Wu, C.-Y. Lee, C.-R. Chen, K.-W. Hsu, and H.-T. Tseng. Optimization of the wind turbine layout and transmission system planning for a large-scale offshore wind

farm by ai technology. *IEEE Transactions on Industry Applications*, 50(3):2071–2080, 2014.

[93] Y. Eroĝlu and S.U. Seçkiner. Design of wind farm layout using ant colony algorithm. *Renewable Energy*, 44:53–62, 2012.

[94] J. Zeng and H. Zhang. Wind speed forecasting model study based on least squares support vector machine and ant colony optimization. *Taiyangneng Xuebao/Acta Energiae Solaris Sinica*, 32(3):296–300, 2011.

[95] S.D.O. Turner, D.A. Romero, P.Y. Zhang, C.H. Amon, and T.C.Y. Chan. A new mathematical programming approach to optimize wind farm layouts. *Renewable Energy*, 63:674–680, 2014.

[96] N. Quan and H. Kim. A tight upper bound for grid-based wind farm layout optimization. volume 2A-2016, 2016.

[97] C.A. Irawan, X. Song, D. Jones, and N. Akbari. Layout optimisation for an installation port of an offshore wind farm. *European Journal of Operational Research*, 259(1):67–83, 2017.

[98] R. Archer, G. Nates, S. Donovan, and H. Waterer. Wind turbine interference in a wind farm layout optimization mixed integer linear programming model. *Wind Engineering*, 35(2):165–175, 2011.

[99] S.-U.-R. Massan, A.I. Wagan, M.M. Shaikh, and R. Abro. Wind turbine micrositing by using the firefly algorithm. *Applied Soft Computing Journal*, 27:450–456, 2015.

[100] R.A. Rivas, J. Clausen, K.S. Hansen, and L.E. Jensen. Solving the turbine positioning problem for large offshore wind farms by simulated annealing. *Wind Engineering*, 33(3):287–298, 2009.

[101] R. Shakoor, M.Y. Hassan, A. Raheem, and N. Rasheed. Wind farm layout optimization using area dimensions and definite point selection techniques. *Renewable Energy*, 88:154–163, 2016.

[102] James Kennedy and Russell Eberhart. Particle swarm optimization. volume 4, pages 1942–1948, 1995.

[103] M. Dorigo and G. Di Caro. Ant colony optimization: A new meta-heuristic. volume 2, pages 1470–1477, 1999.

[104] Today in energy, 2017.

[105] M.Z. Jacobson, C.L. Archer, and W. Kempton. Taming hurricanes with arrays of offshore wind turbines. *Nature Climate Change*, 4(3):195–200, 2014.